멤브레인(Membrane Journal)
Vol. 17, No. 3 September, 2007, 254-268

Na형 Faujasite 제올라이트 분리막 형성 및 CO_2/N_2 분리

조 철 희† · 여 정 구 · 안 영 수 · 한 문 희 · 김 용 하* · 현 상 훈**

한국에너지기술연구원 나노소재연구센터, *부경대학교 화학공학과, **연세대학교 세라믹공학과
(2007년 9월 15일 접수, 2007년 9월 27일 채택)

Secondary Growth of Sodium Type Faujasite Zeolite Layers on a Porous α-Al_2O_3 Tube and the CO_2/N_2 Separation

Churl Hee Cho†, Jeong Gu Yeo, Young Soo Ahn, Moon Hee Han, Yong Ha Kim*, and Sang Hoon Hyun**

Nano Materials Research Center, Korea Institute of Energy Research, Daejeon 305-304, Korea
*Department of Chemical Engineering, Bukyung National University, Pusan 860-739, Korea
**Department of Ceramic Engineering, Yonsei University, Seoul 120-749, Korea
(Received September 15, 2007, Accepted September 27, 2007)

요 약: 다양한 재료특성(Si/Al 몰비, 두께, 구조적 불완전성)을 갖는 Na형 faujasite 제올라이트 분리층을 다공성 α-알루미나 튜브 표면에 수열조건에서 이차성장 시키고 CO_2/N_2 분리거동을 CO_2/N_2 몰비가 1인 혼합기체에 대하여 30°C에서 평가하였다. 수열조건 중에서 수열용액 내의 SiO_2 양은 형성된 제올라이트 분리층의 재료특성에 가장 큰 영향을 주는 변수임을 확인하였다. 즉, 수열용액 내의 SiO_2 양이 증가함에 따라서 형성된 제올라이트 분리층의 Si/Al 몰비, 두께, 구조적 불완전성(discontinuity)은 동시에 증가하였다. 본 논문에서는 불완전한 치밀화에 의해 잔존하는 결정립간 공극(void), GIS Na-P1 상에 의해 형성된 균열(crack) 등 구조적 불완전성이 CO_2/N_2 분리에 가장 큰 영향을 주는 재료특성이며, 투과부에서의 CO_2 탈착이 전체 CO_2 투과의 율속단계(rate-determining step)임을 확인하였다.

Abstract: Sodium type faujasite (FAU) zeolite layers with diverse materials characteristics (Si/Al ratio, thickness, and structural discontinuity) were hydrothermally grown on a porous α-Al_2O_3 tube, and then the CO_2/N_2 separation was evaluated at 30°C for an equimolar mixture of CO_2 and N_2. Among hydrothermal conditions, SiO_2 content in hydrothermal solution seriously affected materials characteristics: with an increment in the SiO_2 content, Si/Al ratio, thickness, and structural discontinuity of grown FAU zeolite layer simultaneously increased. The present study reveals that structural discontinuity (intercrystalline voids due to an incomplete densification and cracks induced by GIS Na-P1 phase) is the most important variable affecting the CO_2/N_2 separation. Also, it was suggested that the CO_2 desorption in permeate side be the rate-determining (slowest) step in the overall CO_2 permeation.

Keywords: *sodium type FAU zeolite membrane, secondary growth, CO_2/N_2 separation, Si/Al ratio, thickness, intercrystalline void, rate-determining step*

1. Introduction

Sodium type FAU zeolite membrane is one of the most noticed zeolite membranes. The increasing attention has been paid due to the promising separation performances in recovering carbon dioxide [1-8], dewatering liquid organics [9-11], and separating organic mixtures [9,12,13]. The excellent separations originate in the large pore diameter (7.4 Å) and the preferential chemical affinity to carbon dioxide, water, and so on.

As reported by several research groups [1-16], sodium type FAU zeolite membrane has been synthesized by the secondary growth process, a heterogeneous

†주저자(e-mail : chcho@kier.re.kr)

growth process under a hydrothermal condition. In the synthesis process, seeds were introduced to surface of a porous support and grow to be a continuous FAU zeolite layer. The terminology "continuous" means that grown zeolite layer is structurally defect-free. But, it is difficult to grow a wide and defect-free FAU zeolite layer through the secondary growth process. Therefore, the reported permeating area was as small as a few cm^2 [1-16]. At a glance, uniform seeding helps to prepare a wide and continuous zeolite membrane. Several seeding processes such as rubbing [1-7], slurry coating [9,12], dip coating [16], and electrophoretic deposition [8] have been introduced. Nonetheless, those seeding processes took too much seeding time and needed careful processing control.

In the secondary growth process, a micrometer-sized FAU zeolite powder has been generally seeded on the surface of a porous α-Al_2O_3 tube or plate with a mean pore diameter of 0.1 to 1 μm. In recent years, there were a few research reports where a nanometer-sized powder has been applied as a seed [16]. Nanoseeds are more advantageous than micrometer-sized ones due to a short inter-spacing between themselves over a porous support. The short inter-spacing gives us a high opportunity to form a thin and continuous layer in a short time. Also, seeds, that are smaller than the mean pore diameter of the porous support, can enter into the internal pores of the porous support in the seeding process. The seed growth in the internal pores gives a good adhesion between the grown zeolite layer and porous support. Unfortunately, a nanometer-sized FAU zeolite powder has been synthesized using a long-term and well-controlled hydrothermal process [16].

In the present study, a brief nanoseed-making process and a simple seeding process were introduced and made the secondary growth process successfully prepare a wide (120 cm^2) FAU zeolite membrane. Also, sodium type FAU zeolite layers with diverse Si/Al ratio, thickness, and discontinuity were grown, and then the CO_2/N_2 separation were investigated. From the results, it was known that the discontinuity was the most important materials characteristics to determine the CO_2/N_2 separation factor and the CO_2 desorption in permeate side is the rate-determining step in the overall CO_2 permeation.

2. Experimental

A seed was prepared from a commercial FAU zeolite powder (HiSiv 1000, UOP, USA) by a combined process of vibratory milling (5400, Red Devil Equipment Co., USA) and centrifugation (Supra 22K, Hanil Science Ind., Korea). In the vibratory milling, α-Al_2O_3 balls with an average diameter of 5 mm and water were used as the milling media and the solvent, respectively. A porous α-Al_2O_3 tube (Ceracomb Co., Korea) was applied as a membrane support. The porosity was 35 vol% and the mean pore diameter was 120 nm. The outer and inner diameters were 10.5 and 7.5 mm, respectively. The support length (L) was 50 to 400 mm, exactly 50, 100, 200, and 400 mm.

The α-Al_2O_3 support was seeded on the outer surface using a vacuum-assisted filtration process. A similar seeding process was also used to prepare LTA (NaA) zeolite membranes [17]. In the seeding process, the interior of support was evacuated at 25 torr for 20 min. During the evacuation, particulate seeds were filtered with the porous α-Al_2O_3 support and uniformly coated on the outer surface.

Zeolite layers were grown over the seeded α-Al_2O_3 support under various hydrothermal conditions. Hydrothermal solutions were made of water glass (193-08185, Wako Pure Chemical Industries Ltd., Japan), sodium aluminate (1923-3260, Showa Chemicals Inc., Japan), sodium hydroxide (39155-0350, Junsei Chemical Co., Ltd., Japan), and water. The composition was Al_2O_3 : SiO_2 : Na_2O : H_2O = x : y : z : 840 in a molar basis, where x was 0.5 to 2, y was 6 to 17 and z was 8 to 18. From now on, the hydrothermal solution with a composition of $x$$Al_2O_3$-$y$$SiO_2$-$z$$Na_2O-840H_2O$ is called (x, y, z, 840) solution. The prepared hydro-

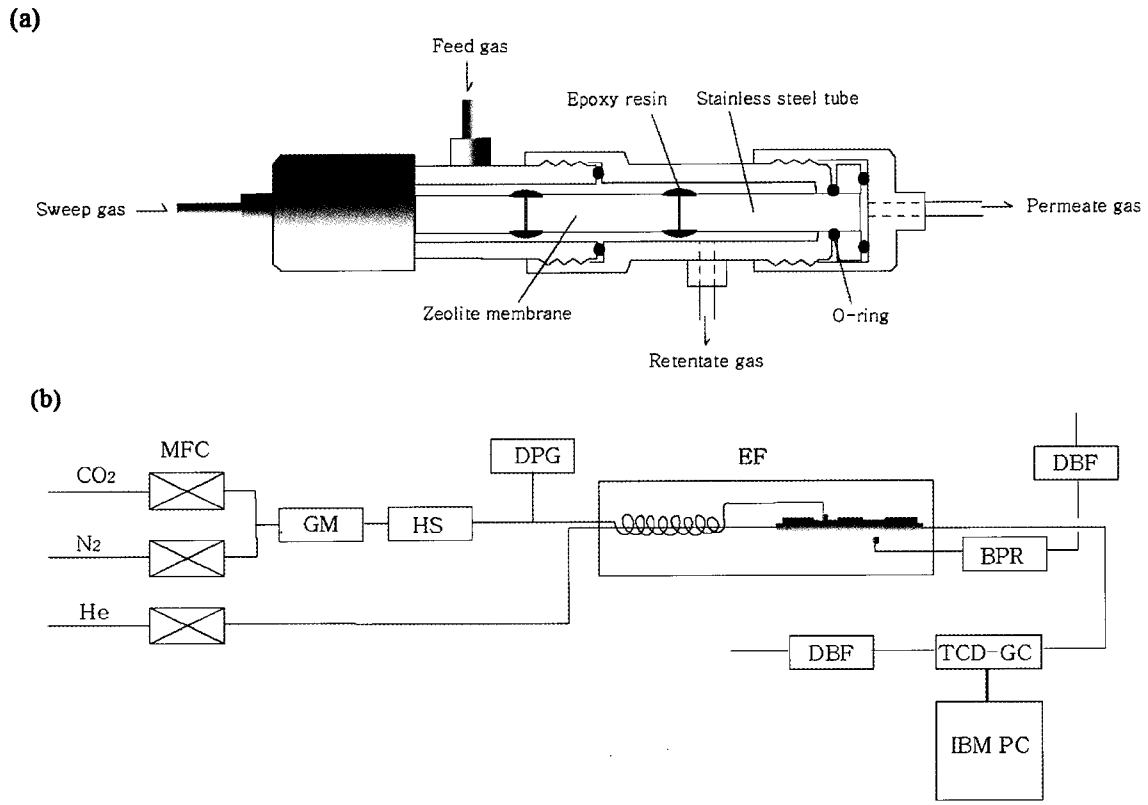

Fig. 1. Schematic diagrams of experimental set-ups for permeation experiments: (a) permeation cell and (b) permeation system.

thermal solution was introduced to a Teflon-made mini-autoclave with a seeded α-Al_2O_3 support. The mini-autoclave was put in a convection oven. The oven temperature (T) was 80 to 120°C and the hydrothermal time (t) was 12 to 24 h.

Crystalline phase and morphology of prepared zeolite membrane were analyzed by X-ray diffractometer (D/max2000-Ultima^{Plus}, Rigaku, Japan) and scanning electron microscopy (S-4700, Hitachi, Japan), respectively. In the SEM analyses, the molar ratio of Si to Al of grown zeolite layer was evaluated by EDS. From now on, the molar ratio of Si to Al molar is called the Si/Al ratio.

Separation of CO_2 and N_2 through a prepared zeolite membrane was evaluated in the He sweeping mode for an equimolar mixed gas of CO_2 and N_2. First, a prepared membrane was installed in a permeation test cell (Fig. 1(a)). The stainless steel tube attaching process with an epoxy resin reduced the permeating membrane length by around 20 mm. The zeolite membrane with a length of 400 mm was cut into two equal-length membranes, and then the average gas permeations were evaluated. Second, the permeation test cell was installed in a permeation test system (Fig. 1(b)). The permeation system has an electric furnace (EF) to control permeation temperature. Prepared membrane installed in the permeation system was cleaned and dehumidified at 80°C for 4 h by flowing He gas in the feed and permeate sides. After the He cleaning, furnace temperature was cooled down to be 30°C, the single permeation temperature of the present study. Third, an equimolar mixture of CO_2 and N_2 was introduced to the feed side. Before the feeding, the equimolar mixed gas had passed through a gas mixer (GM) and a humidity scrubber (HS). The feeding rate was 350 mL/min and the feed pressure was controlled to be 1 to 3 bars with a back pressure regulator (BPR). He sweeping gas was introduced at a flow rate of 0 to

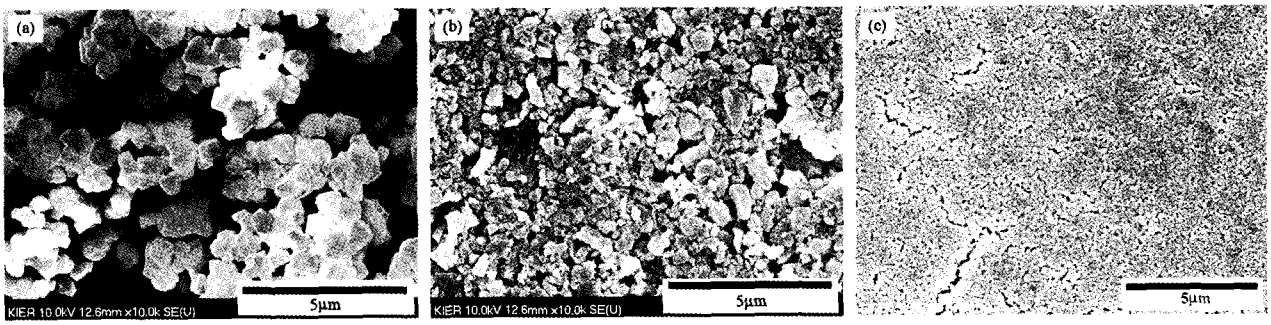

Fig. 2. SEM images for the (a) commercial FAU powder (HiSiv 1000), (b) powder obtained after the vibratory milling, and (c) powder after the centrifugation. The prepared seed was a monodispersed nanometer-sized particle.

200 mL/min and controlled by mass flow controllers (MFC, Bronkhorst, Netherlands).

In the present study, CO_2 and N_2 permeances were calculated with permeating area (A), total permeation rate, molar ratio of CO_2 to N_2 of permeate gases, and partial pressure difference between the feed and permeate sides. Permeating area was calculated by the outer diameter and permeating membrane length. Total permeation rate was simply obtained by subtracting the He sweeping rate from the total gas flow rate in the permeate side. Total gas flow rate in the permeate side was measured by a digital bubble flow meter (DBF). Molar ratio of CO_2 to N_2 in the permeate side was measured by a TCD-GC (ACME 6000, Young Lin Co., Korea). Partial pressures of CO_2 and N_2 in the permeate side was simply calculated from the flow rates of CO_2, N_2 and He. In the calculation, total pressure in the permeate side was assumed to be 1 bar, because the permeate side was open to air. Also, CO_2/N_2 separation factor was identical to molar ratio of CO_2 to N_2 in the permeate side, because feed gas was an equimolar mixed gas of CO_2 and N_2.

3. Results and Discussion

A nanometer-sized seed was prepared from a commercial sodium-type FAU zeolite powder (HiSiv 1000, UOP, USA) using a combination of vibratory milling and centrifugation. Fig. 2 represents SEM images of the (a) commercial powder, (b) powder obtained after vibratory milling, and (c) powder obtained after centrifugation (6,000 rpm). The XRD patterns and LS particle size distributions were shown in Figs. 3(b) to (d) and Figs. 4(a) to (c), respectively. Also, Figs. 3(a) and (e) represent XRD patterns of α-Al_2O_3 supports before and after the seeding process, respectively. Fig. 2(c) and Fig. 4(c) reveal that the prepared seed is a monodisperse nanometer-sized particle with an average diameter of 230 nm. Also, Fig. 3(d) reveals that the prepared nanoseeds are composed of FAU zeolite phase and a considerable amount of α-Al_2O_3 phase. The α-

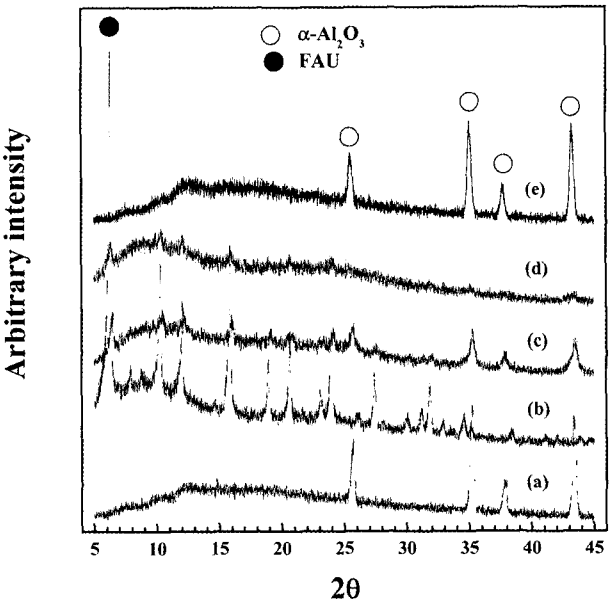

Fig. 3. XRD patterns for the (a) α-Al_2O_3 support, (b) commercial FAU powder (HiSiv 1000), (c) powder obtained after the vibratory milling, (d) powder obtained after centrifugation, and (e) seeded α-Al_2O_3 support. The prepared nanoseed contained a considerable amount of α-alumina phase.

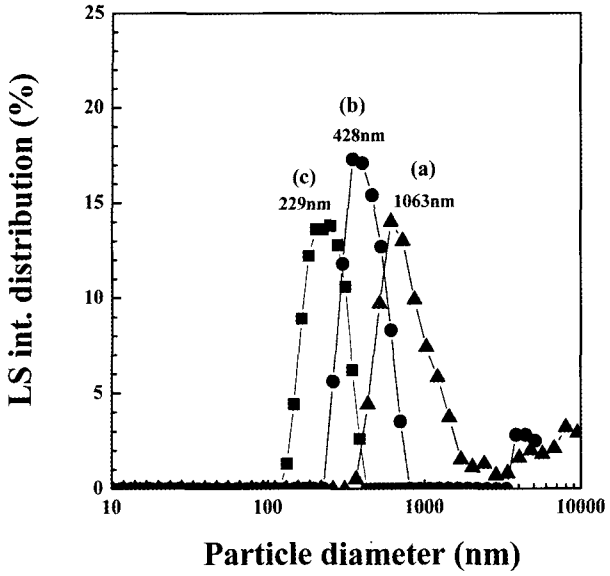

Fig. 4. LS size distributions for the (a) commercial FAU powder, (b) powder obtained after the vibratory milling, and (c) powder obtained after the centrifugation. The mean diameter of the prepared nanoseed was around 230 nm.

Al_2O_3 phase present in the nanoseed was sourced from the α-Al_2O_3 balls introduced in vibratory milling.

Figs. 5(a) to (d) represents SEM images for the surfaces of α-Al_2O_3 supports (a) before and (b) after the seeding, and EDS (c) Si and (d) Al distributions over the seeded support. Considering that the porous support is a pure α-Al_2O_3 phase and the FAU phase in the nanoseed is the single source of Si, the uniform Si distribution (Fig. 5(c)) means that the vacuum-assisted filtration process made a uniform seeding in a short time (20 min).

In the present study, sodium type FAU zeolite layers with diverse Si/Al ratio, thickness, and discontinuity were grown in various hydrothermal conditions.

Fig. 6 represents SEM images for fractured sections of zeolite membranes prepared at various hydrothermal temperature (T) and time (t). The membrane shown in Fig. 6(h) was prepared in the (1, 14, 17, 973) solution and the others were prepared in the (1, 10, 14, 840) solution. As the hydrothermal conditions (T and t) were intensified, the thickness of grown zeolite layer increased to more than 20 μm, even though there was an exception (Fig. 6(e)). In the present study, zeolite layer means top layer composed of polycrystalline zeolite phase. As shown in Fig. 6, a spherical or semi-

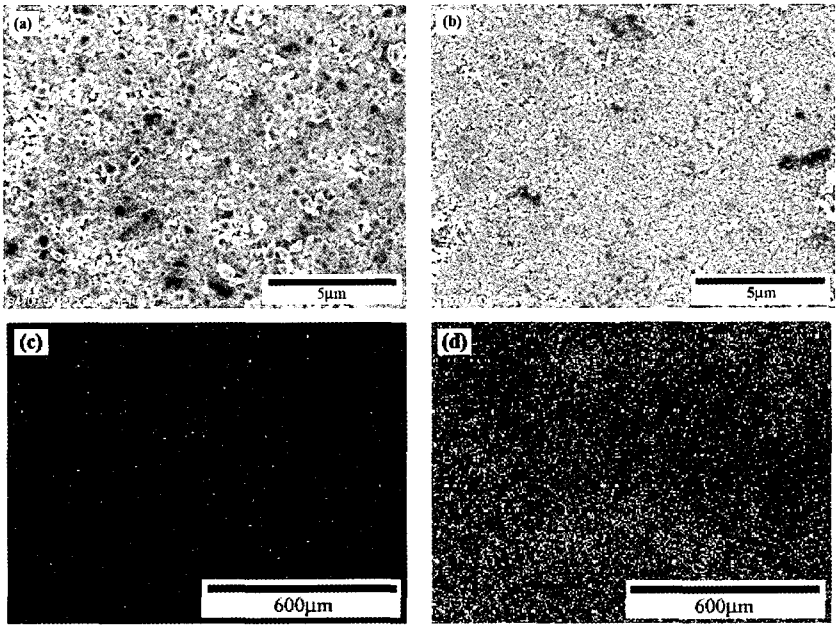

Fig. 5. SEM images for the top views of α-Al_2O_3 supports (a) before and (b) after the seeding, and EDS (c) Si and (d) Al distributions over the seeded α-Al_2O_3 support. The uniform distribution of Si over the seeded support means a uniform seeding.

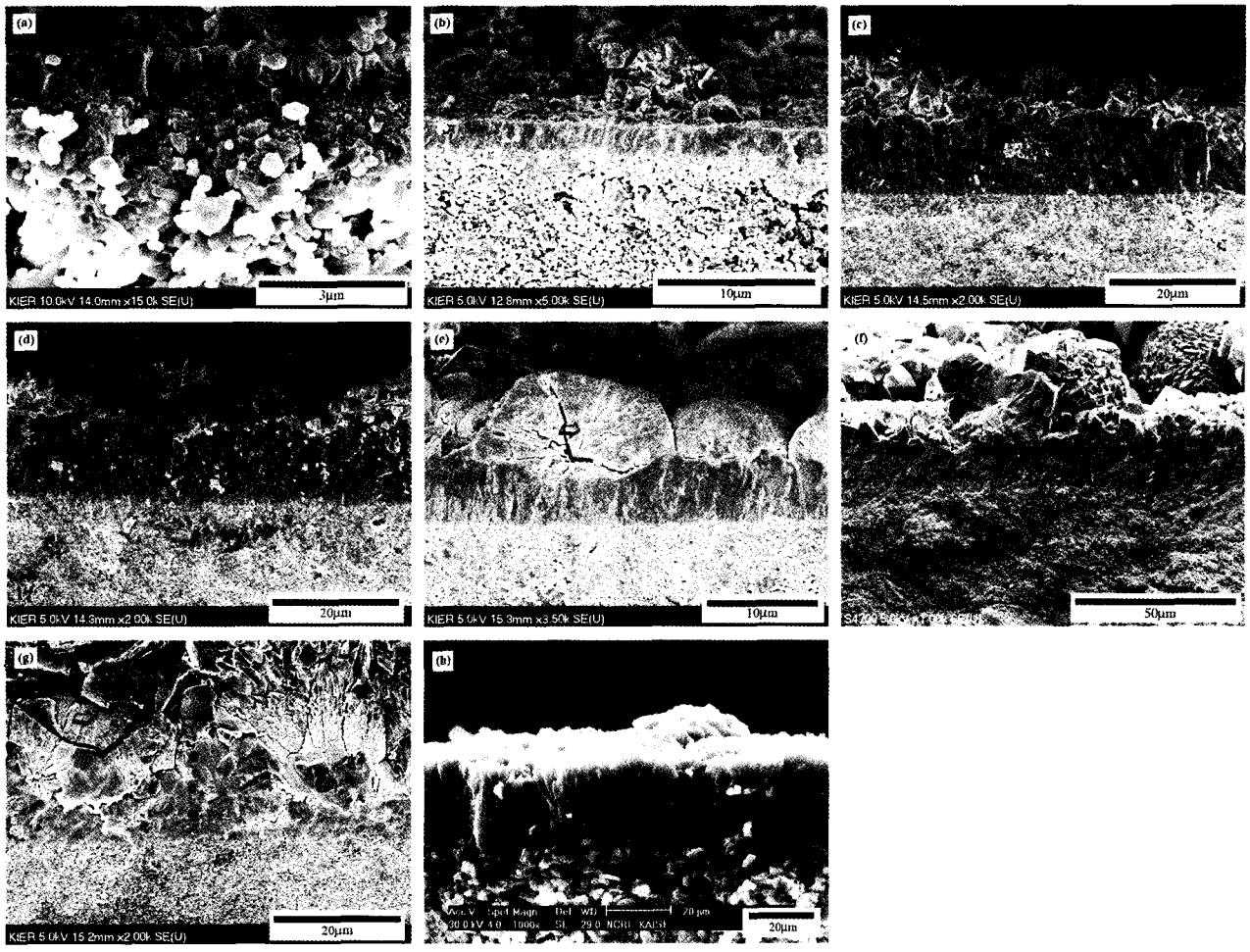

Fig. 6. SEM images for the fractured sections of zeolite membranes prepared at various hydrothermal temperature and time: (a) T = 80°C; t = 12 h, (b) T = 80°C; t = 18 h, (c) T = 80°C; t = 24 h, (d) T = 90°C; t = 24 h, (e) T = 100°C; t = 24 h, (f) T = 110°C; t = 24 h, (g) T = 120°C; t = 24 h, and (h) T = 120°C; t = 24 h.

spherical granule composed of primary crystals was clearly shown over the top layer. The spherical phase was so far as to penetrate into the zeolite layer (Fig. 6(g) and (h)). It is remarkable that the spherical granule contained many well-developed cracks (Fig. 6(e) and (g)). The cracks even penetrate through the zeolite layer (Fig. 6(g)). EDS analyses showed that the Si/Al ratio of formed zeolite layers in Fig. 6(a) to (g) was ranged from 1.4 to 1.6, around 1.5 and the Si/Al ratio of the spherical phase was less than 1.

Fig. 7 represents XRD patterns of zeolite membranes prepared at various hydrothermal temperature and time. All the membranes were prepared by using the (1, 10, 14, 840) solutions. In the zeolite membranes prepared at 110 and 120°C, XRD peaks for GIS Na-P1 zeolite phase were clearly shown. The spherical phase shown in Fig. 6 was GIS Na-P1 zeolite phase. The GIS Na-P1 phase was indicated as arrows in Fig. 6. As mentioned earlier, all the prepared membranes were dehumidified at 80°C for 4 h by flowing He gas in the feed and permeate sides. The cracks induced by GIS Na-P1 phase were generated during the He cleaning process, especially on heating.

Fig. 8 represents CO_2/N_2 separations through zeolite membranes prepared at various hydrothermal temperature and time. All the membranes were prepared by using the (1, 10, 14, 840) solution. All the membrane was with a length of 5 cm. CO_2 permeance was 7 ×

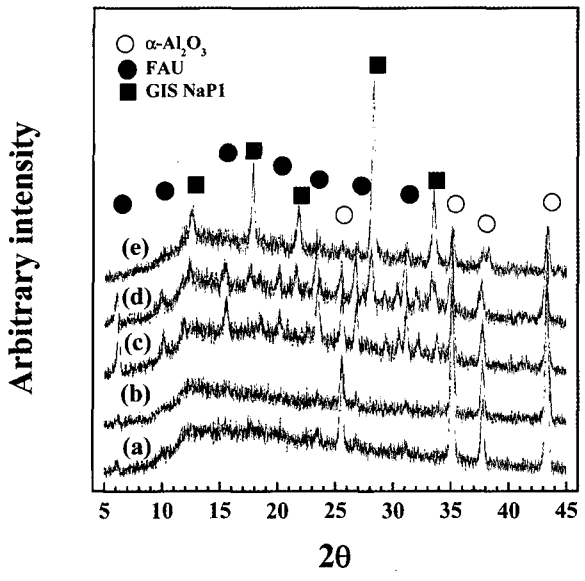

Fig. 7. XRD patterns for zeolite membranes prepared at various hydrothermal temperature and time: (a) T = 80°C; t = 12 h, (b) T = 80°C; t = 18 h, (c) T = 80°C; t = 24 h, (d) T = 110°C; t = 24 h and (e) T = 120°C; t = 24 h.

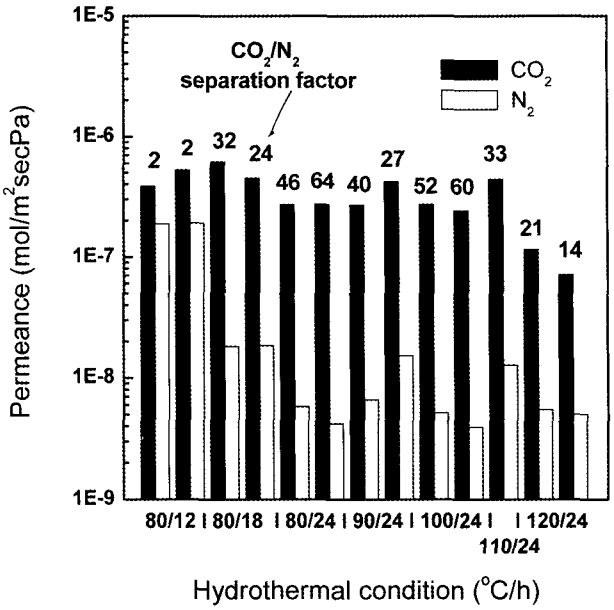

Fig. 8. CO_2/N_2 separations through zeolite membranes prepared at various hydrothermal temperature and time. All the membranes was synthesized in the (1, 10, 14, 840) solution. Filled and open bars were the CO_2 and N_2 permeances, respectively.

10^{-8} to 6.2 × 10^{-7} mol/m^{2}secPa, while N_2 permeance was 4 × 10^{-9} to 1.9 × 10^{-7} mol/m^{2}secPa. N_2 permeance was strongly affected by hydrothermal temperature and time, while CO_2 permeance was insensitive to them. CO_2/N_2 separation factor, ranged from 2 to 64, showed a maximum among zeolite membranes prepared at 80 to 100°C. The dependence of CO_2/N_2 separation faction on hydrothermal condition could be explained by discontinuity of grown FAU zeolite layers. Discontinuity means non-zeolite pores such as intercrystalline voids between adjacent FAU zeolite grains due to an incomplete densification and cracks induced by GIS Na-P1 Phase (Fig. 6(g)). Discontinuity works as a successful path for N_2 permeation, because N_2 gases show relatively weak adsorption on FAU zeolite phase. Therefore, N_2 gases freely make massive flows from the feed side to the permeate side. For FAU zeolite layer to show a good CO_2/N_2 separation, FAU zeolite grains must be sufficiently interlocked between themselves. In other words, thickness of FAU zeolite layer has to be sufficient. In the secondary growth process, intercrystalline voids will be initially interconnected and then remain an isolated one or fully shrink to disappear. The interconnected voids will reduce CO_2/N_2 separation, because those gives channels along that N_2 gases freely flow. Therefore, in Fig. 8, the initial increment in CO_2/N_2 separation factor was due to an increase in continuity with increasing the thickness of FAU zeolite layer, and the later decrease was due to a decrease in continuity due to a presence of cracks induced by GIS Na-P1 phase.

Fig. 9 represents SEM images for fractured sections of zeolite membranes prepared in various hydrothermal solutions. The zeolite membranes shown in Figs. 9(a) to (c) were prepared at 110°C for 24 h and the others were prepared at 80°C for 24 h. SEM morphology and XRD phase analyses revealed that all the prepared zeolite membranes are FAU type phase. Some FAU zeolite membranes have a considerable amount of GIS Na-P1 phase, just put on the FAU zeolite layer (Fig. 9(c)).

The variation in the Al_2O_3 content made little effect on the Si/Al ratio: the Si/Al ratio of the FAU zeolite layers grown in the (***0.5***, 6, 14, 840), (***0.8***, 6, 14, 840)

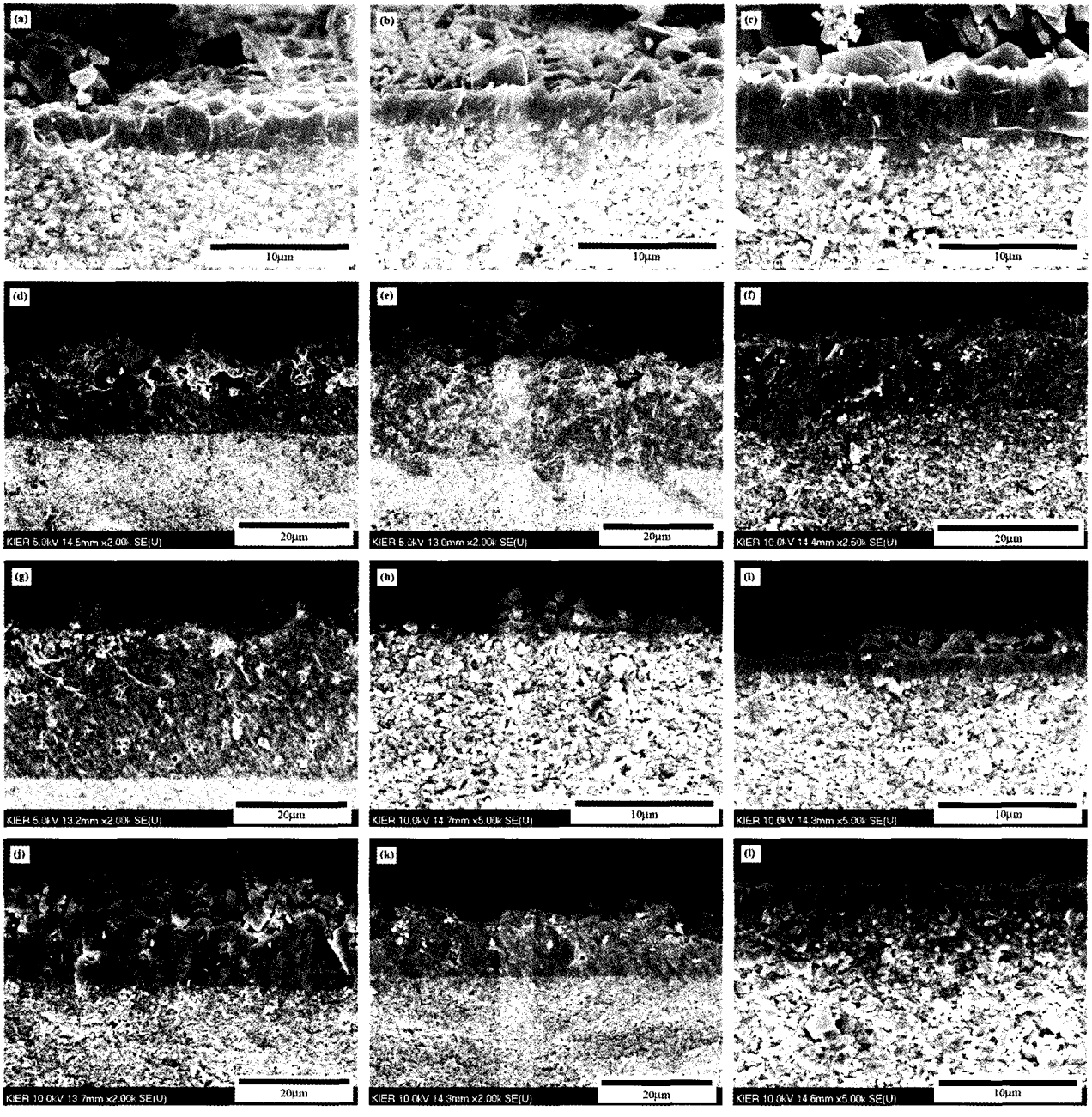

Fig. 9. SEM images for the fractured sections of the zeolite membranes prepared in the (a) (***0.5***, 6, 14, 840), (b) (***0.8***, 6, 14, 840), (c) (***1***, ***6***, 14, 840), (d) (1, ***10***, ***14***, 840), (e) (1, ***13***, 14, 840), (f) (1, ***15***, 14, 840), (g) (1, ***17***, 14, 840), (h) (1, 10, ***8***, 840), (i) (1, 10, ***12***, 840), (j) (1, 10, ***16***, 840), (k) (1, 10, ***18***, 840) and (l) (***0.75***, ***7.5***, 14, 840) solution, respectively.

and (***1***, ***6***, 14, 840) solutions was around 1.3. This phenomenon was reasonable, because there is an unlimited Al_2O_3 source (α-Al_2O_3 support) in the hydrothermal solution. On the other hand, the Si/Al ratio highly depends on the SiO_2 content. Si/Al ratio of FAU zeolite layers grown in (1, ***6***, 14, 840), (1, ***10***, 14, 840), (1, ***13***, 14, 840), (1, ***15***, 14, 840) and (1, ***17***, 14, 840) solutions was 1.31, 1.54, 1.66, 1.76 and 1.94, respectively. SiO_2 content seriously affected Si/Al ratio. The phenomenon was due to an increment in SiO_2 source materials. Si/Al ratio was nearly independent of Na_2O content: the Si/Al ratio of FAU zeolite layers grown in

the (1, 10, ***8***, 840), (1, 10, ***12***, 840), (1, 10, ***14***, 840), (1, 10, ***16***, 840) and (1, 10, ***18***, 840) solutions was around 1.5. Generally, FAU zeolite phase is classified into NaX or NaY type: when the Si/Al ratio is less than 1.5, it is NaX and when the Si/Al ratio is more than 1.5, it is NaY. The FAU zeolite layers grown in the (***0.5***, 6, 14, 840), (***0.8***, 6, 14, 840) and (***1***, 6, 14, 840) solutions were NaX type, while the others are NaY type.

As shown in Fig. 9, thickness of grown FAU zeolite layer seriously depends on Al_2O_3, SiO_2 and Na_2O contents in hydrothermal solution. Thickness increases with increasing Al_2O_3 and SiO_2 contents (Figs. 9(a) to (g)). Larger thickness means faster FAU grain growth rate. Considering that pH value of hydrothermal solutions is around 14, a change in source concentrations is the single reason explaining the increase in FAU grain growth rate. As shown in Fig. 9, SiO_2 content is more effective on thickness than Al_2O_3 content. Al_2O_3 is less soluble than SiO_2 in a strongly basic aqueous solution [18] and there is an unlimited Al_2O_3 source (α-Al_2O_3 support) in hydrothermal solution. Therefore, the minute change of Al_2O_3 content (0.5 to 1) made little effect on FAU grain growth rate, while the change of SiO_2 content (6 to 17) made a significant effect. As shown in Fig. 9(d) and Figs. 9(h) to (k), an increase in Na_2O content increases thickness. In a hydrothermal growth process, sodium hydroxide (NaOH) serves as a mineralizing agent, increasing particle growth rate. Therefore, it is reasonable that thickness increases with Na_2O content. Fig 9(l) represents a SEM image for fractured section of the FAU zeolite membrane prepared in the (***0.75***, ***7.5***, 14, 840) solution. A simultaneous dilution of Al_2O_3 and SiO_2 source effectively reduces thickness.

It is remarkable that intercrystalline voids were clearly shown in the FAU zeolite membranes with relatively large thickness (Figs. 9(d) to (g) and Figs. 9(j) and (k)). The intercrystalline voids were due to an incomplete interlocking induced by a fast grain growth rate. In other words, there was little time for intercrystalline voids to shrink isolated or completely disappear, because a supply route of source materials was hindered by already formed FAU zeolite grains. The intercrystalline voids shown in Figs. 9(d) to (g) and Figs. 9(j) and (k) look like isolated, but are three-dimensionally interconnected. Therefore, the interconnected voids will make a significant reduction in the CO_2/N_2 separation factor, because they role as good paths for N_2 massive flow.

Table 1 represents CO_2/N_2 separations through FAU zeolite membranes grown in various hydrothermal conditions. All the membrane was with a length of 5 cm. In case of the FAU zeolite membranes prepared in the (***0.5***, 6, 14, 840), (***0.8***, 6, 14, 840) and (***1***, 6, 14, 840) solutions, CO_2/N_2 separation factor increased with Al_2O_3 content. The increment in the CO_2/N_2 separation factor was due to an increase in thickness of FAU zeolite layer (Figs. 9(a) to (c)). An increase in the thickness means the continuity. In case of the FAU zeolite membranes grown in the (1, ***10***, 14, 840), (1, ***13***, 14, 840), (1, ***15***, 14, 840) and (1, ***17***, 14, 840) solutions, CO_2 permeance increased and CO_2/N_2 separation factor decreased with an increment in the SiO_2 content. It is difficult to explain why this phenomenon occurs, because a variation in SiO_2 content simultaneously changes Si/Al ratio, thickness, and discontinuity (Figs. 9(d) to (g)). A detailed discussion will be done in next section. In case of the FAU zeolite membranes prepared in the (1, 10, ***8***, 840), (1, 10, ***12***, 840), (1, 10, ***14***, 840), (1, 10, ***16***, 840) and (1, 10, ***18***, 840) solutions, CO_2/N_2 separation factor showed a maximum among the FAU zeolite membrane prepared in the (1, 10, 14, 840) solution. This phenomenon could be explained by the continuity. As shown in Fig. 9(d) and Figs. 9(h) to (k), thickness increased with Na_2O content. Therefore, the initial increase in CO_2/N_2 separation factor was due to an increase in continuity. On the other hand, the later decrease in CO_2/N_2 separation factor was due to a presence of discontinuity, intercrystalline voids (Figs. 9(j) and (k)). The FAU zeolite membrane prepared in the (***0.75***, ***7.5***, 14, 840) solution

Table 1. CO_2/N_2 Separations through FAU Zeolite Membranes Grown in Various Hydrothermal Solutions

Hydrothermal condition					CO_2/N_2 separation		
x (mol)	y (mol)	z (mol)	T (°C)	t (h)	Π (mol/m^{2}secPa) CO_2	N_2	α (CO_2/N_2)
0.5	6	14	110	24	2.6×10^{-7}	1.7×10^{-8}	15
0.8	6	14	110	24	4.4×10^{-7}	1.1×10^{-8}	37
1	6	14	110	24	2.4×10^{-7}	2.9×10^{-9}	82
1	6	14	110	24	3.0×10^{-7}	5.3×10^{-9}	56
1	10	14	80	24	2.7×10^{-7}	5.8×10^{-9}	46
1	10	14	80	24	2.7×10^{-7}	4.2×10^{-9}	64
1	13	14	80	24	4.4×10^{-7}	9.6×10^{-9}	45
1	13	14	80	24	4.3×10^{-7}	8.9×10^{-9}	47
1	15	14	80	24	4.6×10^{-7}	1.1×10^{-8}	40
1	15	14	80	24	4.6×10^{-7}	1.1×10^{-8}	40
1	17	14	80	24	5.3×10^{-7}	2.0×10^{-8}	26
1	17	14	80	24	6.0×10^{-7}	1.6×10^{-8}	36
1	10	8	80	24	5.8×10^{-7}	3.3×10^{-7}	2
1	10	8	80	24	5.3×10^{-7}	3.1×10^{-7}	2
1	10	10	80	24	6.4×10^{-7}	1.5×10^{-7}	4
1	10	10	80	24	6.2×10^{-7}	2.2×10^{-7}	3
1	10	12	80	24	7.1×10^{-7}	6.6×10^{-8}	10
1	10	12	80	24	7.1×10^{-7}	6.8×10^{-8}	10
1	10	16	80	24	4.0×10^{-7}	2.1×10^{-8}	18
1	10	16	80	24	4.7×10^{-7}	2.8×10^{-8}	16
1	10	18	80	24	5.7×10^{-7}	1.4×10^{-7}	4
1	10	18	80	24	3.7×10^{-7}	6.2×10^{-8}	6
0.75	7.5	14	80	24	5.8×10^{-7}	2.0×10^{-8}	27
0.75	7.5	14	80	24	5.2×10^{-7}	1.6×10^{-8}	31

Table 2. CO_2/N_2 Separations through FAU Zeolite Membranes with Diverse Membrane Lengths

Synthesis condition							CO_2/N_2 separation		
L	*A*	*x*	*y*	*z*	*T*	*t*	Π (mol/m^{2}secPa) CO_2	N_2	α (CO_2/N_2)
10	**26.4**	0.75	7.5	14	80	24	3.3×10^{-7}	1.0×10^{-8}	28
10	**26.4**	0.75	7.5	14	80	24	3.3×10^{-7}	9.2×10^{-9}	31
10	**26.4**	0.75	7.5	14	80	24	3.3×10^{-7}	7.4×10^{-9}	39
20	**59.3**	1	10	14	110	24	1.2×10^{-7}	4.0×10^{-9}	26
20	**59.3**	1	10	14	110	24	1.5×10^{-7}	7.1×10^{-9}	19
20	**59.3**	1	10	14	110	24	7.1×10^{-8}	1.7×10^{-9}	40
40	**118.6**	0.8	8	14	80	24	2.3×10^{-7}	1.2×10^{-8}	16

shows a good CO_2/N_2 separation, even though the thickness is small (Fig. 9(l)).

The CO_2/N_2 separation data (Fig. 8 and Table 1) revealed that the FAU zeolite membranes prepared in the present study showed a relatively good CO_2/N_2 separation, comparable to those reported by others [1-8]. This means that the nanoseed and the seeding process applied in the present study are useful in preparing a continuous FAU zeolite membrane. As a confirmation experiment, FAU zeolite membranes with diverse lengths (100, 200, and 400 mm) were prepared and then the CO_2/N_2 separations were evaluated. Table 2 represents detailed synthesis conditions and CO_2/N_2 separations. FAU zeolite membranes with large permeating lengths show relatively good CO_2/N_2 separations. This reconfirms that the nanoseed and seeding processes used in the present study improved the membrane reproducibility in the secondary growth process.

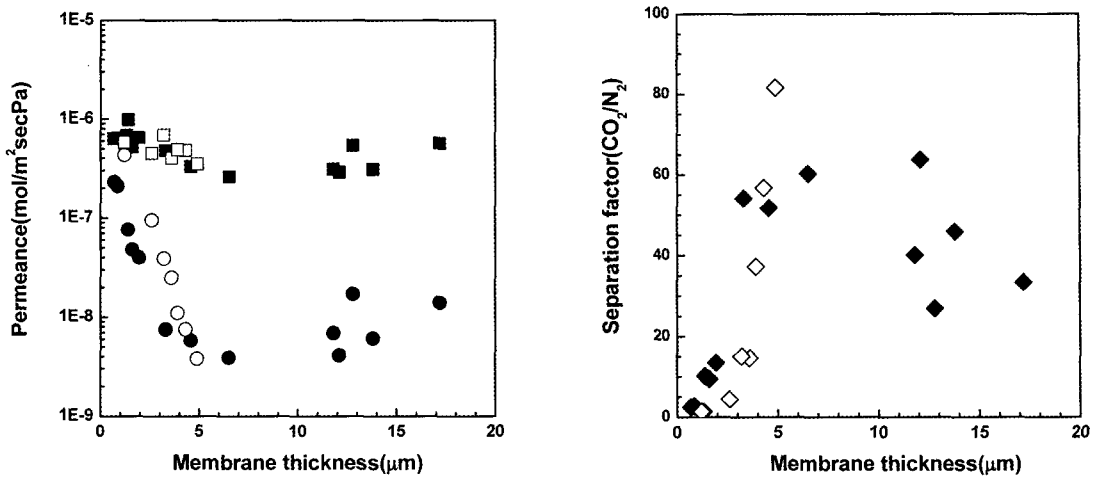

Fig. 10. Gas permeances and separation factor of FAU zeolite membranes with diverse membrane thickness: (a) CO_2 (■, □) and N_2 (●, ○) permeances and (b) CO_2/N_2 separation factor (◆, ◇). Open and closed symbols are separation data for the FAU zeolite membranes with Si/Al ratios of 1.32 and 1.54, respectively.

Generally, in a membrane separation, permeance seriously depends on thickness of separation layer, because it has to penetrate across the layer. Fig. 10 represents (a) CO_2 and N_2 permeances and (b) CO_2/N_2 separation factors through FAU zeolite layers with diverse thickness. In the regime I, an increase in thickness decreased CO_2 and N_2 permeances. Especially, N_2 permeance showed an abrupt decreasing behavior, so that CO_2/N_2 separation factor sharply increased with thickness. This could be explained by an increase in the continuity with increasing the thickness. J. Motuzas *et al.* have suggested that the thickness has to be more than 5 μm, in order to limit the influence of non-zeolite pores [19]. Their suggestion well coincides with the present result. On the other hand, in the regime II, CO_2/N_2 separation factor abruptly decreased with increasing thickness. This phenomenon could be explained by a decrease in the continuity, a presence of intercrystalline voids (Figs. 9(d) to (g) and Figs. 9(j) and (k)). Also, CO_2/N_2 separation data through the membranes with a Si/Al ratio of around 1.3 were included as squares in Fig. 10. The change in Si/Al ratio didn't make a significant effect on CO_2/N_2 separation.

It is generally accepted that CO_2 and N_2 permeations through a FAU zeolite membrane are governed by surface and micropore diffusions, respectively [2]. Therefore, CO_2 permeation through a FAU zeolite membrane is a series reaction composed of three subreactions: CO_2 adsorption in feed side, CO_2 surface diffusion through micropore channel, and CO_2 desorption in permeate side. It is interesting that in the CO_2/N_2 separation data (Figs. 8 and 10 and Table 1), CO_2 permeance is little dependent on the thickness and discontinuity. This means that CO_2 surface diffusion through micropore channel is not the rate-limiting (slowest) step in the CO_2 permeation. On the contrary, CO_2 adsorption in feed side or CO_2 desorption in permeate side might be more important step in the overall CO_2 permeation.

Table 3 represents CO_2/N_2 separations at various feed pressure and He sweeping rate through a FAU zeolite layer whose thickness and Si/Al ratio were around 5 μm and 1.67. The increase in the feed pressure (1 to 3 bars) little increased the CO_2 and N_2 fluxes and decreased the CO_2/N_2 separation factor. An increase in feed pressure means an increase in CO_2 adsorption in feed side. It is interesting that CO_2 flux is nearly independent of feed pressure. This means that CO_2 adsorption in feed side isn't the rate-limiting step in the CO_2 permeation through a FAU zeolite membrane. In other words, the feed pressure of 1 to 3 bars

Table 3. CO_2/N_2 Separations at Various Feed Pressures and He Sweeping Rates through a FAU Zeolite Membrane

Permeation condition		CO_2/N_2 separation		
Feed pressure (bar)	He sweeping rate (mL/min)	J (mol/m^{2}sec)		α (CO_2/N_2)
		CO_2	N_2	
1	146	2.1×10^{-2}	6.1×10^{-4}	33
1.5	146	2.1×10^{-2}	6.2×10^{-4}	34
2	**146**	2.5×10^{-2}	7.6×10^{-4}	33
2.5	146	2.6×10^{-2}	8.9×10^{-4}	30
3	146	2.6×10^{-2}	9.9×10^{-4}	26
2	**0**	1.0×10^{-2}	8.5×10^{-4}	12
2	**26**	2.0×10^{-2}	7.7×10^{-4}	26
2	**51**	2.2×10^{-2}	8.1×10^{-4}	28
2	**100**	1.9×10^{-2}	6.9×10^{-4}	27
2	**191**	3.3×10^{-2}	1.1×10^{-3}	31

sufficiently supplies CO_2 molecules to the mouth of micropore channel. Also, the ignorable dependency of CO_2 flux on the feed pressure has an important engineering meaning that the CO_2 recovery capacity in a FAU zeolite membrane system isn't a function of feed pressure. On the other hand, as shown in Table 3, the increase in the He sweeping rate sharply increased the CO_2 flux, while little changed the N_2 flux. An increase in He sweeping rate will improve CO_2 desorption rate on the exit of micropore channel in permeate side. On the other hand, an increase in He sweeping rate doesn't change N_2 desorption rate because N_2 has low chemical affinity on FAU zeolite phase. Therefore, it is suggested that CO_2 desorption in permeate side is the rate-limiting step in the CO_2 permeation through a FAU zeolite membrane.

The Si/Al ratio was known to have a considerable effect on the CO_2/N_2 separation [4,7]. K. Kusakabe *et al.* [4] have prepared the FAU zeolite membranes with diverse Si/Al ratio (1.06 to 2.18) and then reported that with an increase in the Si/Al ratio, the CO_2 permeance increased while the CO_2/N_2 separation factor decreased. They found that GIS zeolite phase was formed over the FAU zeolite layer with the Si/Al ratio of 1.06. The strong dependency of the CO_2/N_2 separation on the Si/Al ratio was explained by the formation of the GIS zeolite phase over the FAU zeolite layer, because GIS zeolite phase has much smaller pore diameter (4.5 Å × 3.1 Å) than FAU zeolite phase (7.4 Å). Also, K. Kusakabe *et al.* [7] have made a different suggestion that the phenomenon be from the change of micropore structure with a variation of the Si/Al ratio. The explanation was supported by the fact that the CO_2 equilibrium adsorption decreased with the Si/Al ratio.

As shown in Table 1, the same result was shown in the present study. As the SiO_2 content in hydrothermal solutions increased, the CO_2 permeance increased and the CO_2/N_2 separation factor decreased. As shown in Figs. 9(d) to (g), there was no GIS Na-P1 phase over the FAU zeolite layer. Therefore, the phenomenon couldn't be explained by the formation of a continuous GIS Na-P1 layer over FAU zeolite layer. Even though a continuous GIS Na-P1 phase forms over FAU zeolite layer, the effect will be ignorable because cracks will be formed in GIS Na-P1 and FAU zeolite layers (Fig. 6(g)).

The suggestion that a change in the Si/Al ratio induces a change in the micropore structure seems to be reasonable, according to a recent report [19]. Fig. 11 represents (a) a schematic view of sites I, I', II and III that sodium ions can be located in a FAU zeolite phase and (b) the occupancies of sodium ions in FAU zeolite phases with diverse Si/Al ratios, respectively [20].

As the Si/Al ratio increases from 1 to 2.5, the occupancies of sodium ions at sites I' and III decreases, the occupancy at sites II remains constant, and the occupancy at sites I increases. Sites I and I' are located inside the hexagonal prisms and sodalite cages, respectively, so that the effects on CO_2 adsorption would be ignorable. On the other hand, sites II and III are located on the surfaces of FAU supercage, so that the effects on CO_2 adsorption would be considerable. The increase of the Si/Al ratio makes the occupancy at site III decrease and doesn't change that at sites II. Therefore, the increase of the Si/Al ratio would decrease the CO_2 equilibrium adsorption. The CO_2 ad-

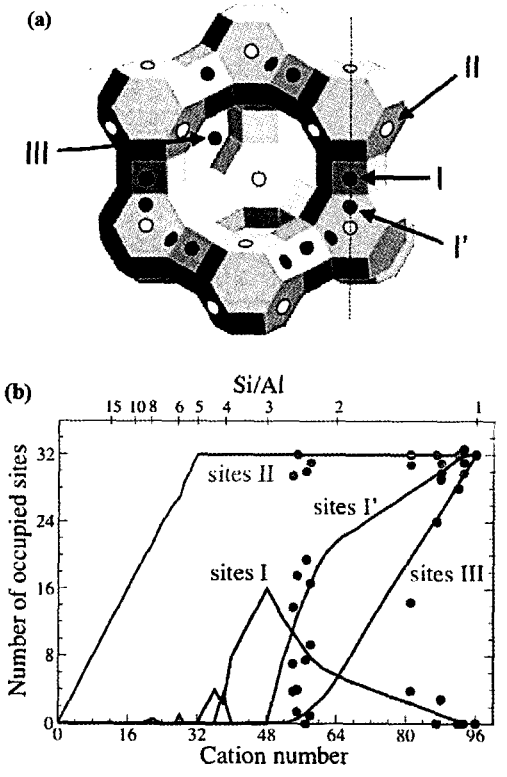

Fig. 11. (a) Schematic view of site I, I', II and III that sodium ions can be located in a FAU zeolite phase and (b) the occupancies of sodium ions in FAU zeolite phases with diverse Si/Al ratios [19].

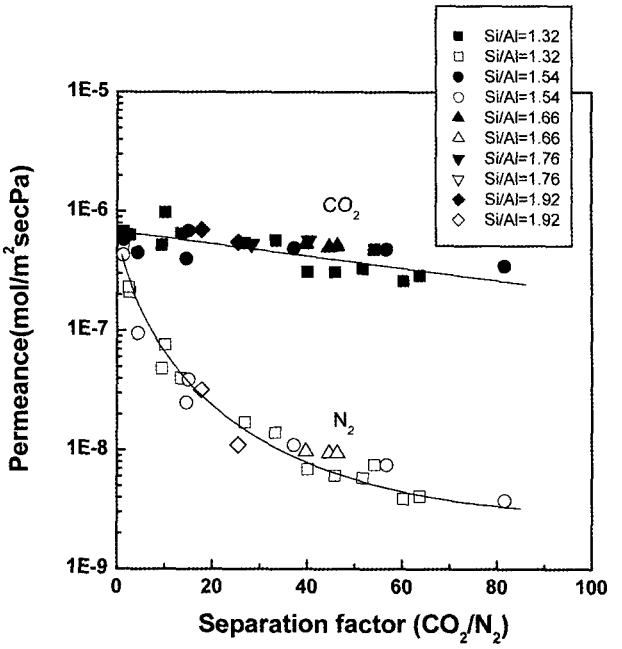

Fig. 12. Trade-off relationships of permeances and CO_2/N_2 separation factor for FAU zeolite membranes with diverse Si/Al ratio: (■, □) 1.32, (●, ○) 1.54, (▲, △) 1.66, (▼, ▽) 1.76, and (◆, ◇) 1.94. The closed and open symbols are for the CO_2 and N_2 permeances, respectively. The variation of Si/Al ratio was not sufficient to free from the relationship.

sorption data reported by others [7] reveal that the increase of the Si/Al ratio reduces the CO_2 equilibrium adsorption. As mentioned earlier, it is acceptable that CO_2 and N_2 permeations through a FAU zeolite membrane are governed by surface and micropore diffusions, respectively [2]. Therefore, the reduction of occupancy at sites III with an increase in the Si/Al ratio would increase the N_2 permeance due to an increment of the apparent micropore diameter and decrease the CO_2/N_2 separation factor.

But, the above-mentioned explanation about the effect of the Si/Al ratio on the CO_2/N_2 separation is not sufficient to explain the variation in the CO_2/N_2 separation as a function of the SiO_2 content (Table 2), because as shown in Figs. 9(d) to (g), the SiO_2 content simultaneously changes the Si/Al ratio, membrane thickness, and discontinuity. As mentioned earlier, the membrane thickness makes a positive effect on the CO_2/N_2 separation: the CO_2/N_2 separation factor increases with an increase in the membrane thickness as shown in the regime I of Fig. 10. The influence of the SiO_2 content on the CO_2/N_2 separation couldn't be explained by the variation of the membrane thickness, because the CO_2/N_2 separation factor decreased with the increase in the membrane thickness (Table 1).

Fig. 12 represents relationships between permeances and separation factor for FAU zeolite membranes with diverse Si/Al ratio. There was a clear tradeoff relationship between permeance and separation factor. It is clearly shown that the variation in the Si/Al ratio (1.3 to 1.9) was not enough to deviate from the relationship. This means that the Si/Al ratio doesn't make a significant effect on the CO_2/N_2 separation. Therefore, the discontinuity such as intercrystalline voids and cracks is the single factor to explain the influence of the SiO_2 content on the CO_2/N_2 separation. For inter-

crystalline voids to be isolated or fully shrink to disappear in the secondary growth process, the FAU grain growth rate should be decelerated.

4. Conclusions

Sodium-type FAU zeolite membrane with diverse materials characteristics were prepared and then the CO_2/N_2 separation were evaluated. From the experimental results, as-followings were known. The continuous FAU zeolite membrane with a permeating area of $\sim 120cm^2$ was successfully synthesized. This means that the nanoseed and the vacuum-assisted filtration process used in the present study improve the membrane reproducibility. The discontinuity such as the intercrystalline voids due to an incomplete interlocking between FAU zeolite grains and the cracks induced by the GIS Na-P1 zeolite phase is more important factor than the Si/Al ratio and membrane thickness. Therefore, the control of the discontinuity should be the top priority in FAU zeolite membrane preparations. The little dependence of the CO_2 permeance on the membrane thickness and discontinuity suggests that the CO_2 surface diffusion through the micropore channel be not the rate-limiting (slowest) step in the CO_2 permeation through a FAU zeolite membrane. On the other hand, the strong dependency of CO_2/N_2 separation on the He sweeping rate means that the CO_2 desorption in the permeate side is the rate-limiting step in the CO_2 permeation.

Acknowledgements

This research was supported by a grant (DB2-201) from Carbon Dioxide Reduction & Sequestration Research Center, one of the 21st Century Frontier Programs funded by the Ministry of Science and Technology of Korean government.

References

1. K. Kusakabe, T. Kuroda, A. Murata, and S. Morooka, "Formation of a Y-type zeolite membrane on a porous α-alumina tube for gas separation", *Ind. Eng. Chem. Res.*, **36,** 649 (1997).
2. Y. Hasegawa, K. Kusakabe, and S. Morooka, "Effect of temperature on the gas permeation properties of NaY-type zeolite formed on the inner surface of a porous support tube", *Chem. Eng. Sci.*, **56**, 4273 (2001).
3. K. Kusakabe, T. Kuroda, K. Uchino, Y. Hasegawa, and S. Morooka, "Gas permeation properties of ion-exchanged faujasite-type zeolite membranes", *AIChE J.*, **45**, 1220 (1997).
4. K. Kusakabe, T. Kuroda, and S. Morooka, "Separation of carbon dioxide from nitrogen using ion-exchanged faujasite-type zeolite membranes formed on porous support tube", *J. Membr. Sci.*, **148** , 13 (1998).
5. Y. Hasegawa, K. Watanabe, K. Kusakabe, and S. Morooka, "The separation of CO_2 using Y-type zeolite membranes ion-exchanged with alkali metal cations", *Sep. Purif. Technol.*, **22-23**, 319 (2001).
6. Y. Hasegawa, K. Watanabe, K. Kusakabe, and S. Morooka, "Influence of alkali cations on permeations properties of Y-type zeolite membranes", *J. Membr. Sci.*, **208**, 415 (2002).
7. Y. Hasegawa, T. Tanaka, K. Watanabe. B. Jeong, K. Kusakabe, and S. Morooka, "Separation of CO_2-CH_4 and CO_2-N_2 systems using ion-exchanged FAU-type zeolite membranes with different Si/Al ratios", *Korean J. Chem. Eng.*, **19(2)**, 309 (2002).
8. K. Weh, M. Noack, I. Sieber, and J. Caro, "Permeation of single gases and gas mixtures through faujasite-type molecular sieve membranes", *Micopor. Mesopor. Mater.*, **54**, 27 (2002).
9. H. Kita, T. Inoue, H. Asamura, K. Tanaka, and K. Okamoto, "NaY zeolite membrane fro the pervaporization separation of methanol-methyl *tert*-butyl ether mixtures", *Chem. Commun.*, 45 (1997).

10. I. Kumakiri, T. Yamaguchi, and S. Nakao, "Preparation of zeolite A and faujasite membranes from a clear solution", *Ind. Eng. Chem. Res.*, **38**, 4682 (1999).
11. H. Jeon, H. Ahn, I. Song, H. Jeong, S. Lee, and Y. Lee, "Separation of water from aqueous isopropyl alcohol solution using NaY zeolite membrane", *Membrane Journal*, **17(1)**, 61 (2007).
12. H. Kita, K. Fuchida, T. Horita, H. Asamura, and K. Okanoto, "Preparation of faujasite membranes and their permeation properties", *Sep. Purif. Technol.*, **25**, 261 (2001).
13. V. Nikolakis, G. Xomeritakis, A. Abibi, M. Dickson, M. Tsapatsis, and D. G. Vlachos, "Growth of a faujasite-type zeolite membrane and its application in the separation of saturated/unsaturated hydrocarbon mixtures", *J. Membr. Sci.*, **184**, 209 (2001).
14. S. Nair, Z. Lai, V. Nikolakis, G. Xomeritakis, G. Bonilla, and M. Tsapatsis, "Separation of close-boiling hydrocarbon mixtures by MFI and FAU membranes made by secondary growth", *Micropor. Mesopor. Mater.*, **48**, 219 (2001).
15. T. Seiko, M. Matsuda, and M. Miyake, "Fabrication of Y-type zeolite films by electrophoretic deposition", *Solid State Ionics*, **151**, 123 (2002).
16. M. Lassinantti, J. Hedlund, and J. Sterte, "Faujasite-type films synthesized by seeding", *Micropor. Mesopor. Mater.*, **38**, 25 (2000).
17. A. Huang, Y. S. Lin, and W. Yang, "Synthesis and Properties of A-type Zeolite Membranes by Secondary Growth Method with Vacuum Seeding", *J. Membr. Sci.*, **245**, 41 (2004).
18. S. Goto, K. Akazawa, and M. Daimon, "Solubility of Silica-Alumina Gels in Different pH Solutions - Discussion on the Hydration of Slags and Fly Ahses in Cement", *Cem. Concr. Res.*, **22**, 1216 (1992).
19. J. Motuzas, A. Julbe, R. D. Noble, A. van der Lee, Z. and J. Beresnevicius, "Rapid synthesis of oriented silicalite-1 membranes by microwave-assisted hydrothermal treatment", *Micropor. Mesopor. Mater.*, **92**, 250 (2006).
20. C. Beauvais, A. Boutin, A. H. and Fuchs, "Adsorption of Water in Zeolite Sodium-faujasite A Molecular Simulation Study", *C. R. Chimie*, **8**, 485 (2005).